

## Two Algorithms for Use with an Orthogonal-View Coded-Aperture System

R. G. Paxman, W. E. Smith, and H. H. Barrett

Arizona Health Sciences Center, Tucson, Arizona

**The goal of single photon emission computerized tomography is to map out a three-dimensional distribution of a radionuclide that is concentrated in a structure of interest. There are a number of imaging modalities that achieve this goal with varying degrees of success. In this study, computer simulation is used to explore a novel imaging modality, orthogonal-view coded-aperture imaging. Furthermore, a comparison is made between two reconstruction algorithms, one being an iterative back-projection algorithm and the other a Monte Carlo algorithm. Finally, evidence is presented suggesting that a deficiency in the projection data due to multiplexing is less disturbing than that due to limited angular range.**

J Nucl Med 25: 700-705, 1984

We have known for some time that coded-aperture imaging can be used to encode tomographic information (1). However, most attempts to exploit this property of coded apertures have focused on single-view geometries, namely, those using a single, planar-coded aperture. Such schemes collect projection data confined to a limited angular range. It has become increasingly evident that this kind of limitation in the data set is almost impossible to overcome (2). In contrast, Lefkopoulos et al. (3) recently reported favorable reconstructions using an orthogonal-view coded-aperture system in which each of the two orthogonal-coded apertures consisted simply of two pinholes. Figure 1 depicts such an imaging system in which a more complex pinhole-coded aperture has been substituted for the two-pinhole apertures. Other investigators have examined similar orthogonal-view systems (4-6).

The reconstruction task here is ambitious, since we seek to reconstruct a three-dimensional distribution from a two-dimensional data set, namely, the coded images. This is tantamount to trying to solve for  $N^3$  unknowns with  $N^2$  equations. A second kind of deficiency in the data is due to the overlap of the various pinhole projections (Fig. 2). In the region of overlap, the data are mixed or "multiplexed" so that it is no longer possible to know through which pinhole a given photon passed. It is hoped that these deficiencies can be overcome in part with the use of prior knowledge about the object.

Despite the problems associated with these data deficiencies, the orthogonal-view coded-aperture system offers several advantages.

1. There is no detector motion in this scheme, so that all of the

data can be acquired simultaneously. Such a system is a natural candidate for dynamic studies.

2. It is well known that coded apertures are capable of much higher photon-collection efficiencies than collimators. For certain objects this may permit lower dose or exposure time (1,7,8).

3. Because the data include projections over a wide range of view angles, the severe artifacts associated with limited-angle imaging schemes are avoided.

4. The imaging geometry is well suited to the use of modular cameras (Milster TD, et al., unpublished data).

In order to simplify the simulations, the dimensionality of the problem was reduced by collapsing the vertical dimension. Instead of reconstructing a three-dimensional distribution, a two-dimensional distribution was sought from a one-dimensional data set. Figure 3 illustrates this collapsed geometry, which was the imaging modality we explored by computer simulation. Note that an essential feature of the three-dimensional case was maintained: depth information was sought from a dimensionally deficient data set.

The reconstruction grid used in the simulations contained  $64 \times 64$  pixels, while the detector arrays had 256 elements in each of the two views. The ratio of object elements to be reconstructed to detector elements was 8:1. The one-dimensional coded aperture was a uniformly redundant array (URA) of eight pinholes, the same array being used in each of the two orientations (9).

The reconstructions were performed by two fundamentally different algorithms, which are individually described in the next two sections. Following this, these two algorithms are compared. Finally, a comparison is made between reconstructions using multiplexed data and reconstructions using limited-angle data.

### ITERATIVE BACK-PROJECTION

It is convenient to express the formation of the coded image in operator notation:

Received Sept. 29, 1983; revision accepted Dec. 22, 1983.

For reprints contact: R. G. Paxman, Dept. of Radiology, Div. of Nucl. Med., Arizona Health Sciences Center, Tucson, AZ 85724.

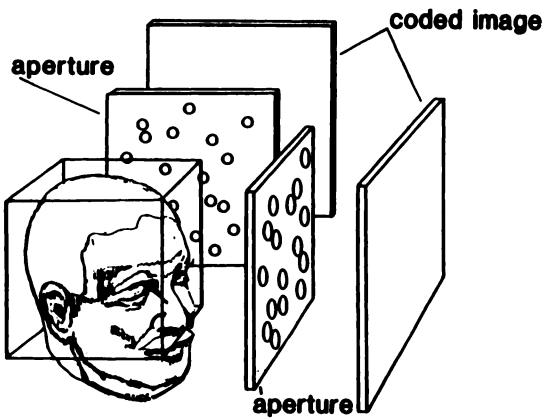


FIG. 1. Proposed orthogonal-view coded-aperture system. Overlapping pinhole projections of object on detector surfaces form coded image.

$$g = P(f),$$

where  $f$  is the two-dimensional true object and  $g$  is the one-dimensional coded image representing the data set. The operator  $P$  is a generalized projection operator. In the case of a multiple-pinhole coded aperture,  $P$  corresponds to projecting each object point through each of the pinholes to the detector plane.

For a first estimate of the original object, we could simply back-project the coded images through the coded aperture. The operation of back-projection, which we represent by the symbol  $B$ , is illustrated pictorially in Fig. 4. The result (Fig. 5a) is a blurred version of the original object (Fig. 6a) in which the space-variant point spread function is shown in Figs. 5b & 5c. The combined operations of projection followed by back-projection, are then, equivalent to a single blurring operation.

$$\text{1st estimate: } \hat{f}_1 = BP(f)$$

This first estimate obviously needs further processing. One approach is to perform deblurring with the iterative Jacobi algorithm (10). By blurring the latest estimate and comparing this with a blurred version of the object, a correction term is formed that can be added to the latest estimate to create a new estimate:

$$K + 1 \text{ estimate: } \hat{f}_{K+1} = \hat{f}_K + \alpha[\hat{f}_1 - BP(\hat{f}_K)].$$

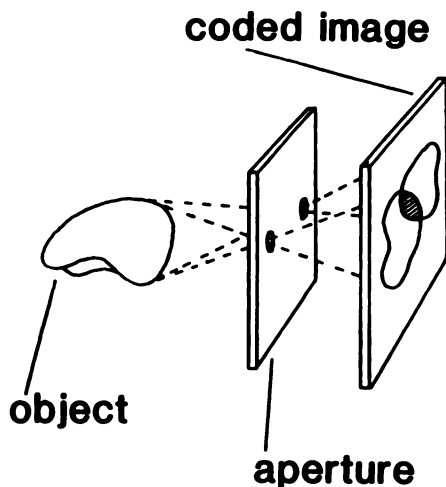


FIG. 2. Multiplexing of data. In region where projections overlap, it is not possible to know through which pinhole given photon passed.

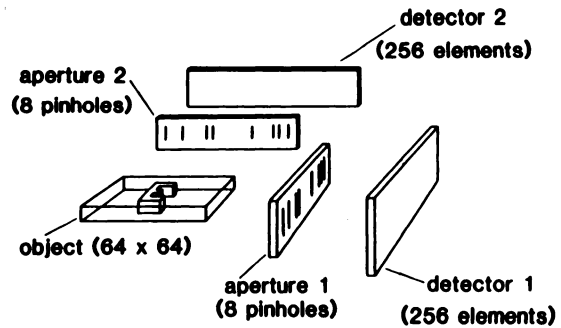


FIG. 3. Geometry for simulations. Vertical dimension has been collapsed so that task is to restore two-dimensional depth information from one-dimensional coded images.

Here  $\alpha$  is an acceleration parameter that affects the rate of convergence of the algorithm.

This algorithm is similar in spirit to the well-known ART and SIRT algorithms used in computed tomography. Both ART and SIRT algorithms can be interpreted in terms of discrete projection and back-projection applied iteratively. The Jacobi algorithm, however, updates the projection of the latest estimate only once per iteration, whereas this is not true of either ART or SIRT algorithms.

There are some desirable features associated with the iterative approach.

1. By truncating the iterative process appropriately, noise amplification is suppressed.

2. This approach provides a computationally straightforward way of handling a space-variant imaging problem.

3. Most importantly, the algorithm provides a convenient framework for enforcing prior knowledge at each iteration. For example, it is known in advance that the distribution of radionuclides must be a positive quantity. Therefore, a constraint is applied that forces each intermediate reconstruction to be positive. In addition to the positivity constraint, we can enforce a constraint implying knowledge of the outer boundary of the object. Reconstructions with and without these constraints are shown in Fig. 6. The convergence of this simulation is shown in Fig. 7.

#### A MONTE CARLO APPROACH: SIMULATED ANNEALING

Reconstruction was also performed by a Monte Carlo algorithm that is completely different in character from the more conventional iterative back-projection approach. This second method models the reconstruction procedure as an optimization problem in which the cost function describes how well the reconstruction

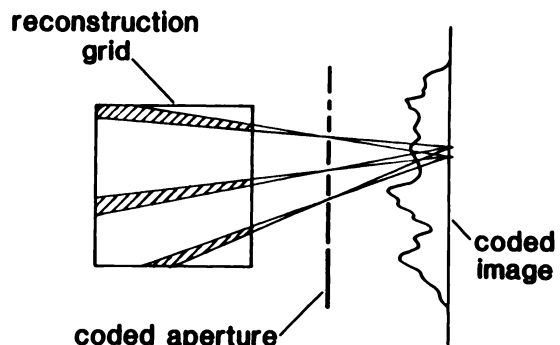
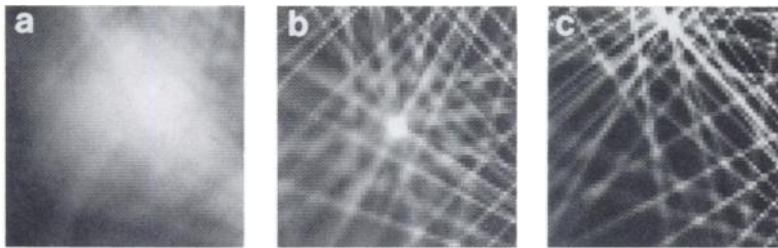


FIG. 4. Back-projection step. Shown is back-projection of single detector element in coded image.



**FIG. 5.** First estimate of object. (a): First estimate of object is blurred version of true object. (b): Space-variant blur function is shown for point in center of field. (c): Space-variant blur function is shown for point at edge of field.

agrees with the data (coded images) while conforming to the constraints. We define the cost function or "energy" of an object estimate as the RMS difference between its coded image and the true object's coded image, namely, the original data. The latest object estimate is constructed by adding or subtracting single "grains" of brightness to the earlier estimate in a random fashion (Fig. 8). Grains that decrease the energy of the system are always accepted. However, in order to avoid getting trapped in local minima, the algorithm also accepts some grains that actually increase the energy according to the Boltzmann probability law, borrowed from statistical mechanics. The probability that a grain producing a change in energy  $\Delta E$  will be accepted is given formally by:

$$P(\Delta E) = \begin{cases} e^{-\Delta E/KT} & \Delta E \geq 0 \\ 1 & \Delta E < 0 \end{cases}$$

where T = effective temperature of the system  
 K = Boltzmann's constant.

The effective temperature can be thought of as a parameter of the algorithm subject to program control. The temperature is slowly reduced in stepwise fashion, allowing the energy at each step to achieve a type of "thermodynamic equilibrium" so that the total energy fluctuates about some mean value. Premature freezing of estimates is avoided by reducing the temperature slowly in this fashion. Because this procedure mimics the annealing process used in the production of solid-state materials, the algorithm has been called simulated annealing (11-13).

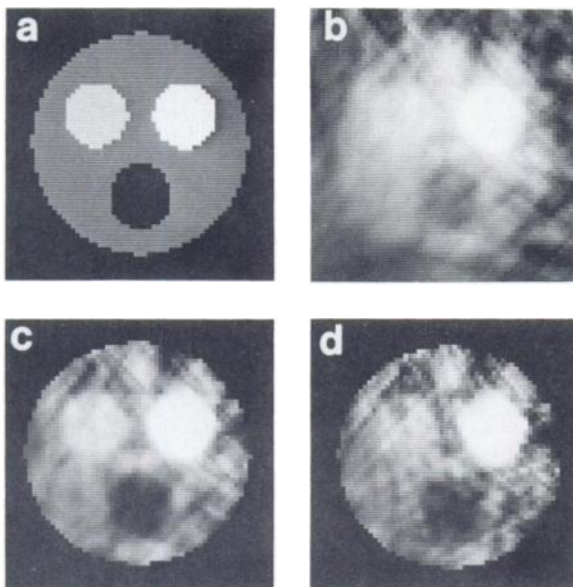


**FIG. 6.** Reconstructions with iterative back-projection. (a): True object. (b): Unconstrained reconstruction after 50 iterations. (c): Reconstruction with knowledge of object's outer boundary, and positivity constraint enforced at each iteration. (d): Constrained reconstruction in which 3% Poisson noise (at signal peak) has been added to coded images.

Monte Carlo algorithms have the attractive feature that they are extremely flexible (14). Details of the imaging process such as attenuation, pinhole vignetting, and scattering are easily incorporated into the algorithm. It is also easy to enforce prior knowledge constraints throughout the reconstruction. Positivity is enforced by simply not accepting any grains that would imply negative values in the reconstruction. An additional smoothing constraint is incorporated by generalizing the definition of the energy to include spatial correlation of nearest neighbor pixels in the reconstruction. Figure 9 shows several reconstructions derived with simulated annealing.

COMPARISON OF ALGORITHMS

The reconstructions presented in the previous two sections are surprisingly good, considering the severe data deficiencies involved. It is clear that tomographic imaging is possible with the orthogonal-view system. Figure 10 illustrates typical cross sections from two reconstructions, showing that the reconstructions are quantitatively accurate.

We turn now to the comparison of the two algorithms, where it appears that both algorithms perform the reconstruction task well. The simulated annealing reconstructions seem qualitatively to have a slight edge over those reconstructed through iterative back-projection. Simulated annealing also seems to "find" the outer boundary of the object without the aid of constraints better than iterative back-projection, although the reasons for this are elusive. The real strength of the simulated-annealing approach lies in its extreme flexibility. The iterative back-projection is the faster of the two algorithms, taking approximately 1 hr to produce a reconstruction on a PDP 11/34 minicomputer, whereas the simulated-annealing algorithm takes close to 8 hr on this machine. The simulated-annealing algorithm has also been implemented on a VAX 780, which has cut the reconstruction time to 10 min. We are currently putting both algorithms on an array processor to further enhance computing speeds.

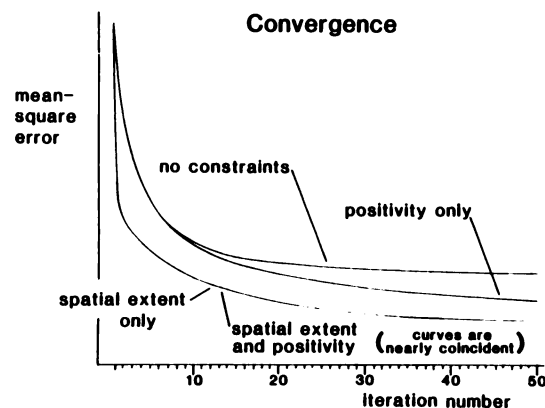


**FIG. 7.** Convergence of iterative back-projection algorithm. Mean-square errors between true object and its estimate are plotted as function of iteration number.

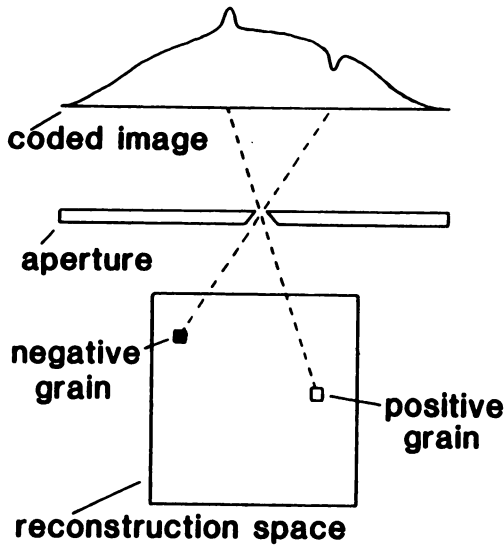


**FIG. 8.** Adding “grains” to reconstruction. Coded image of current object estimate is perturbed by adding or subtracting grains of brightness to object estimate. For clarity, only one pinhole in coded aperture is shown.

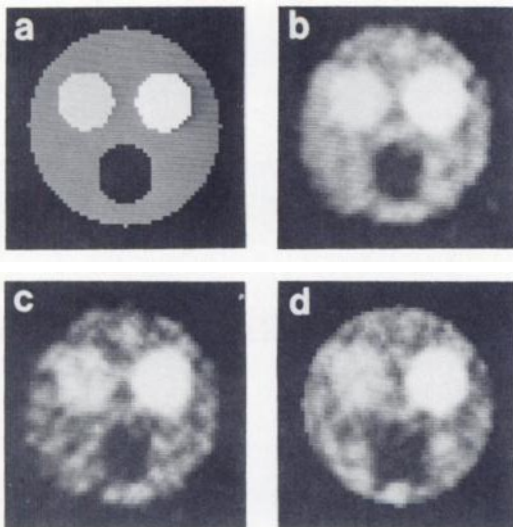


**FIG. 9.** Reconstructions with simulated annealing. (a): True object. (b): Reconstruction after testing 300,000 grains. (c): Reconstruction from coded images with 3% Poisson noise (at signal peak). Again, 300,000 grains were tested. (d) Reconstruction in which both attenuation and noise (3% at signal peak) have been included in simulation. An additional constraint of knowledge of outer boundary was enforced, and 500,000 grains were tested.

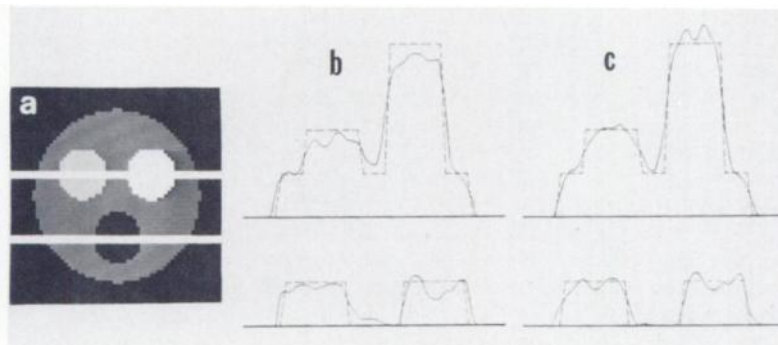


**FIG. 10.** Cross sections of reconstructions. (a): Object showing location of cuts. Cross sections shown were made by averaging three adjacent horizontal lines. (b): Cross sections of iterative back-projection reconstruction. (c) Cross sections of simulated annealing reconstruction.

The real criterion for judging the success of an algorithm is the ability to reconstruct an estimate that conforms to the a priori constraints with the data. Both algorithms perform well in this regard. When no noise is present in the data, either algorithm produces an object estimate whose coded image  $\hat{I}$  differs from the true coded image  $I$  by less than 1.3%, that is

$$\frac{\text{RMS}(I-\hat{I})}{\text{RMS}(I)} < 1.3\%$$

where RMS refers to root mean square. This is well within random noise fluctuations that would appear in a clinical study. The success with which both algorithms achieve agreement with the data suggests that the imaging task explored here is largely independent of algorithm. For this reason we believe that significant improvement in the reconstructions will be achieved, not by fine-tuning algorithms, but by optimizing the design of the coded apertures and the geometry of the imaging system.

LIMITED ANGLE COMPARED WITH MULTIPLEXING

Next we compare the effect of taking data over a limited range of angles with that of multiplexing. If one were to open each pinhole in the aperture one at a time and store its projection separately, then the effects of multiplexing would be removed. There would be no overlap of projections and therefore no mixing of data. Such a procedure closely resembles classical SPECT imaging except that the projections now have a fan-beam geometry. If now the sequentially opened pinholes were confined to only one of the two orthogonal apertures, we would have classical SPECT data over a limited angular range. The data would be free of any deficiency due to multiplexing, but would be deficient in the angular range of projections available. This case has been extensively explored in the literature (15-16). It is interesting to compare this case with the one in which a wide range of angles is available but multiplexing degrades the data. The latter corresponds to the orthogonal-view coded-aperture imaging system described in this paper. The comparison is made in Fig. 11, which presents strong evidence that a deficiency in the data due to multiplexing is tolerated more easily than that due to limited angular range.

A final and more realistic comparison involves introducing random noise due to the radioactive nature of the source into the simulations. Now the two cases (unmultiplexed compared with multiplexed) are compared when the total data acquisition time is held constant. For the unmultiplexed case, only one pinhole projection is recorded at a given time. The amount of time each pinhole is open is given by  $T/N$  where  $T$  is the total data acquisition time and  $N$  is the number of pinholes per aperture. In this case the noise at the signal peak of the projection data is about 10.5%. By contrast, the multiplexed case allows all projections to be recorded throughout the entire data acquisition period, resulting in 3.0% noise at the signal peak of the coded image. The results are shown in Fig. 12. It is clear from these reconstructions that the multi-

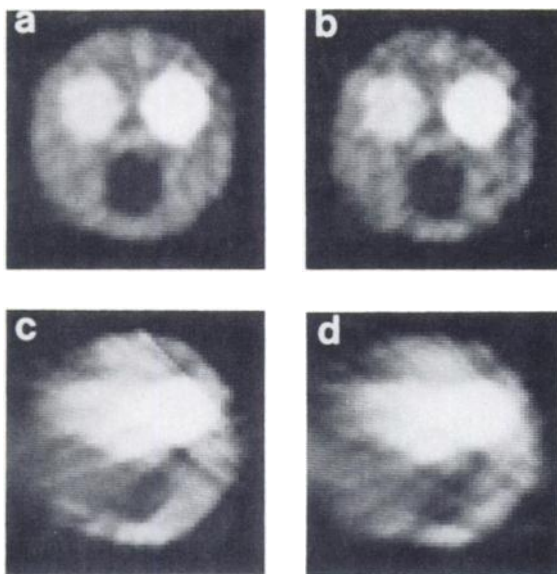


**FIG. 11.** Limited angle compared with multiplexing. (Reconstruction by way of simulated annealing). (a): Orthogonal view unmultiplexed. (b): Orthogonal view multiplexed. (c): Single view unmultiplexed. (d): Single view multiplexed.

plexed case is less susceptible to degradation in the reconstructions due to photon noise. This is because  $N$  times as many photons are collected in the multiplexed case as in the unmultiplexed case.

One might argue that this comparison underestimates the number of photons that could be collected in the unmultiplexed case since, for a given object, certain pairs of pinhole projections may not overlap and could therefore be recorded simultaneously. However, in order to know which pairs of projections don't overlap, one needs some knowledge about the extent of the object in advance. We believe that the comparison is reasonable when the extent of the object is not known beforehand.

#### SUMMARY AND CONCLUSIONS

The orthogonal-view, coded-aperture system presented here has potential as an imaging system for SPECT in clinical use. The system is particularly promising for doing dynamic studies, where detector motion can be a serious drawback. The simulations performed indicate that this system is able to restore tomographic information successfully. The orthogonal-view system is much more successful than its single-view counterpart because projections can be obtained over a much wider angular range. This concept is not limited to a strict orthogonal-view design, and we are working on multiple-view, coded-aperture systems in which several coded apertures view an organ of interest from a variety of orientations.

In recent years there has been much interest in the problem of tomography with projection data from a limited angular range. The system presented bypasses this seemingly insurmountable problem, but it introduces the problem of multiplexing. We have presented evidence that the effects of multiplexing are tolerated much more easily than the effects of limiting the angular range of the projection data. This is particularly true when the random nature of the source is introduced into the simulations, and the total data acquisition time is held constant.

Finally, two fundamentally different reconstruction algorithms have been compared. Both successfully give reconstructions consistent with the data and the constraints. Qualitatively, the reconstructions given by both algorithms are similar, suggesting that

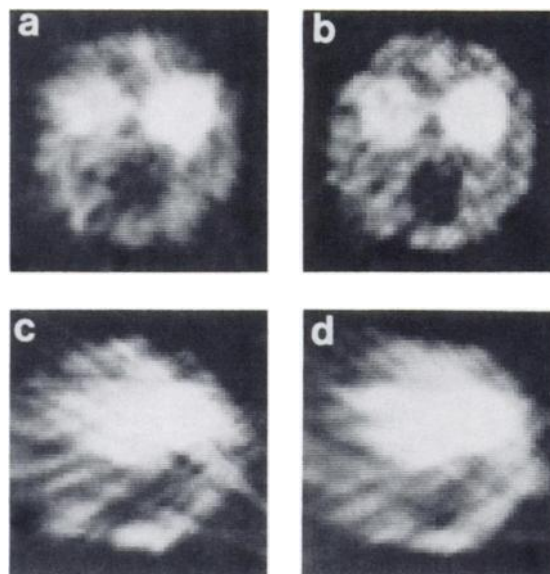


**FIG. 12.** Limited angle compared with multiplexing with statistical considerations. (Reconstruction by way of simulated annealing). (a): Orthogonal view unmultiplexed. (b): Orthogonal view multiplexed. (c): Single view unmultiplexed. (d): Single-view multiplexed.

the imaging task studied here is largely independent of algorithm. We are working on the optimization of the coded-aperture design with respect to a given class of objects. It is hoped that an optimized system will be able to restore the clinically most important features of objects within the class of interest. In addition, we are pursuing phantom studies as well as simulations that model the full three-dimensional case.

#### ACKNOWLEDGMENTS

We acknowledge the significant efforts of Gene R. Gindi, who initiated the research leading to this investigation. We are also grateful to D. Lefkopoulos and J. Fonroget for pointing out the potential for improved imaging associated with the orthogonal-view geometry. This research was supported by the National Cancer Institute through grant No. CA 23417.

#### REFERENCES

1. BARRETT HH, SWINDELL W: *Radiological Imaging: Theory of Image Formation, Detection, and Processing*. New York, Academic Press, 1981, Chap. 8
2. DAVISON ME: The ill-conditioned nature of the limited angle Tomography Problem. *SIAM J Appl Math* 43:2, 428-448, 1983
3. LEFKOULOPOULOS D, FONROGET J, DEVAUX JY, et al: Quantitative 3D imaging with coded apertures by using SVD decomposition of the transmission matrix. In *Proceedings of the Third World Congress of Nuclear Medicine and Biology*. Raynaud C, ed. Paris, Pergamon, 1982, pp 503-506.
4. GINDI GR: Reconstruction of a two-dimensional slice from its one-dimensional coded image. In *Technical Report TR83/03*. Division of Imaging Sciences, Dept. of Diagnostic Radiology, Yale University, New Haven, CT, 1983
5. STEINBACH A: An analysis of the depth resolution problem in one-dimensional coded aperture imaging. Ph.D. Thesis, Dept. of Applied Physics, Stanford University, Stanford, CA, 1977
6. TIPTON MD: The ODCAT: one dimensional coded aperture

- tomography. *Proc. Soc. Photo-Opt Instrum Eng* 152 p 113-120, 1978
7. SIMPSON RG, BARRETT HH: Coded-aperture imaging. In *Imaging in Diagnostic Medicine*, Nudelman S, Patton D, eds. New York, Plenum, 1980, Chap. 8
  8. METZ CE, BECK RN: Quantitative effects of stationary linear image processing on noise and resolution of structure in radionuclide images, *J Nucl Med* 15, p. 164-170 (1974)
  9. WILD WJ: Dilute uniformly redundant sequences for use in coded aperture imaging. *Opt Lett* 8:247-249, 1983
  10. GINDI GR: Use of *a priori* information for improved tomographic imaging in coded-aperture systems. Ph.D. Thesis, University of Arizona, Tucson, AZ, 1982
  11. SMITH WE, BARRETT HH, PAXMAN RG: Reconstruction of objects from coded images by simulated annealing. *Opt Lett* 8:4, 199-201, 1983
  12. KIRKPATRICK S, GELATT CD J, VECCHI MP: Optimization by simulated annealing. *Science* 220:671-680, 1983
  13. METROPOLIS N, ROSENBLUTH A, ROSENBLUTH M, et al: Equation of state calculations by fast computing machines, *J Chem Phys* 21, 1087-1092, 1953
  14. DUNN WL: Inverse monte carlo analysis, *J Comp Phys* 41, 154-166, 1981
  15. GARNERO L: Tomographic imaging with limited view angle using an expansion on a set of eigenfunctions adapted to space limited objects. *J Opt Soc Am* in press
  16. TAM KC, PEREZ-MENDEZ V: Tomographic imaging with limited-angle input. *J Opt Soc Am* 71, 582-592, 1981